Two-Meter Temperature and Precipitation from Atmospheric Reanalysis Evaluated for Alaska

RICK LADER

Department of Atmospheric Sciences, Geophysical Institute, and International Arctic Research Center, University of Alaska Fairbanks, Fairbanks, Alaska

UMA S. BHATT

Department of Atmospheric Sciences, Geophysical Institute, University of Alaska Fairbanks, Fairbanks, Alaska

JOHN E. WALSH

International Arctic Research Center, University of Alaska Fairbanks, Fairbanks, Alaska

T. SCOTT RUPP

International Arctic Research Center, and Scenarios Network for Alaska and Arctic Planning, University of Alaska Fairbanks, Fairbanks, Alaska

PETER A. BIENIEK

International Arctic Research Center, University of Alaska Fairbanks, Fairbanks, Alaska

(Manuscript received 11 June 2015, in final form 7 December 2015)

ABSTRACT

Alaska is experiencing effects of global climate change that are due, in large part, to the positive feedback mechanisms associated with polar amplification. The major risk factors include loss of sea ice and glaciers, thawing permafrost, increased wildfires, and ocean acidification. Reanalyses, integral to understanding mechanisms of Alaska's past climate and to helping to calibrate modeling efforts, are based on the output of weather forecast models that assimilate observations. This study evaluates temperature and precipitation from five reanalyses at monthly and daily time scales for the period 1979–2009. Monthly data are evaluated spatially at grid points and for six climate zones in Alaska. In addition, daily maximum temperature, minimum temperature, and precipitation from reanalyses are compared with meteorological-station data at six locations. The reanalyses evaluated in this study include the NCEP–NCAR reanalysis (R1), North American Regional Reanalysis (NARR), Climate Forecast System Reanalysis (CFSR), ERA-Interim, and the Modern-Era Retrospective Analysis for Research and Applications (MERRA). Maps of seasonal bias and standard deviation, constructed from monthly data, show how the reanalyses agree with observations spatially. Cross correlations between the monthly gridded and daily station time series are computed to provide a measure of confidence that data users can assume when selecting reanalysis data in a region without many surface observations. A review of natural hazards in Alaska indicates that MERRA is the top reanalysis for wildfire and interior-flooding applications. CFSR is the recommended reanalysis for North Slope coastal erosion issues and, along with ERA-Interim, for heavy precipitation in southeastern Alaska.

1. Introduction

In the past 60 years the average annual surface temperature in Alaska has warmed by 1.7°C (3°F), and temperatures are projected to increase by as much as

Corresponding author address: Rick Lader, International Arctic Research Center, University of Alaska Fairbanks, P.O. Box 752325, Fairbanks, AK 99775.
E-mail: rtladerjr@alaska.edu

DOI: 10.1175/JAMC-D-15-0162.1

5.6°C (10°F) by the end of the twenty-first century (Chapin et al. 2014). Alaska has warmed more, and is warming at a faster rate, than any other region in the United States. This situation is due in part to polar amplification, which is characterized by positive feedback mechanisms in the climate system (Bekryaev et al. 2010; Pithan and Mauritsen 2013). Given the magnitude of the recent and expected future change in Alaska, it is necessary to model past and future climate scenarios with the best available observational information.

For Alaska, this is a problematic task. There are only 20 first-order weather stations that are routinely maintained by National Weather Service personnel although Alaska is the largest state in the country. There are many other cooperative stations, but they are typically insufficient for climate research because the periods of record are short or have numerous gaps. Much of the ''usable data'' can be unreliable. For example, a large percentage of the precipitation that falls across Alaska is snow, which is difficult to measure accurately, particularly in windy conditions (Yang et al. 1998).

Reanalysis models help to bridge this data gap. Reanalysis is a high-spatiotemporal-resolution gridded meteorological data product that is made by assimilating past observations into a physically consistent weather forecast model. Each analysis cycle begins by using a previous forecast as a background field or ''first guess.'' The background field is then interpolated to the location of an assimilated observation, and the difference between this estimate and the value of the observation is the analysis increment (Kalnay 2003). The analysis increment is added onto the background field with appropriate weighting measures, and a new analysis is produced. The reanalysis cycle is typically 6 or 12 h. There are multiple reanalysis datasets available globally or regionally, and therefore an evaluation for Alaska would help to inform impact studies that use these data.

Reanalysis has been used to investigate many processes that are important for Alaska. The Pacific decadal oscillation was linked with downstream atmospheric signals for North America by using pressure and temperature data from the National Centers for Environmental Prediction–National Center for Atmospheric Research reanalysis (hereinafter R1; Kalnay et al. 1996) by Mills and Walsh (2013). Other Alaska-relevant studies have used R1 to study the impacts of the Aleutian low (Hartmann and Wendler 2005; Rodionov et al. 2005; Pickart et al. 2009; Shulski et al. 2010), El Niño (Bieniek et al. 2011), and boreal fire dynamics (Rupp et al. 2007).

An ocean wave model in the southeastern Chukchi Sea was forced with winds from the North American Regional Reanalysis (NARR; Mesinger et al. 2006) to determine historical wave heights (Francis and Atkinson 2012). The largest contribution to sea level rise from melting glaciers and ice caps in the Northern Hemisphere (excluding Greenland) was determined to be from Alaska (Mernild et al. 2014), on the basis of a study that used atmospheric forcing from the Modern-Era Retrospective Analysis for Research and Applications (MERRA) reanalysis (Bosilovich 2008).

For broader study, including the pan-Arctic region, Smith et al. (2014) developed an Internet-based reanalysis intercomparison tool to allow data users to easily map and analyze time series and the differences between models. Brönnimann et al. (2012) noted that temperature agreement between multiple datasets in the Arctic is highest in the midtroposphere and is considerably weaker at the surface. Fan et al. (2008) compared a high-resolution experimental reanalysis product with R1 and the precursor model to ERA-Interim, ERA-40 (Uppala et al. 2005), and found that ERA-40 generally performed the best, although the experimental dataset was nearly as skillful.

Reanalyses provide a valuable service to the climate community, but each reanalysis has its own strengths and weaknesses. The relatively low amount of data that is assimilated into the reanalyses at far-northern latitudes makes the output datasets more dependent on the background forecast model. An understanding of each reanalysis—the data assimilation, the forecast model, and the changes to the observing systems involved—is essential prior to selecting the best available dataset for an end user's application.

To address these needs, this study evaluates near-surface air temperature and precipitation from five reanalyses for Alaska on both daily and monthly scales over a 31-yr period from 1979 to 2009. This study uniquely helps to answer the following questions:

1) How do the mean, variance, and extremes of temperature and precipitation from the reanalyses compare to each other and to station data (and other observational information) for Alaska?
2) In areas void of long-term station data in Alaska, what are the preferred reanalyses?
3) Are there applications for which some reanalyses produce more useful output than others?

Study region

This study includes all of Alaska, and the spatial analyses compartmentalize the state into climate zones, which represent a logical amalgamation of the 13 original Alaskan climate divisions (Fig. 1a) developed by Bieniek et al. (2012) using cluster analysis. The predominant vegetation type, climate, and extreme events that are characteristic of each zone are as

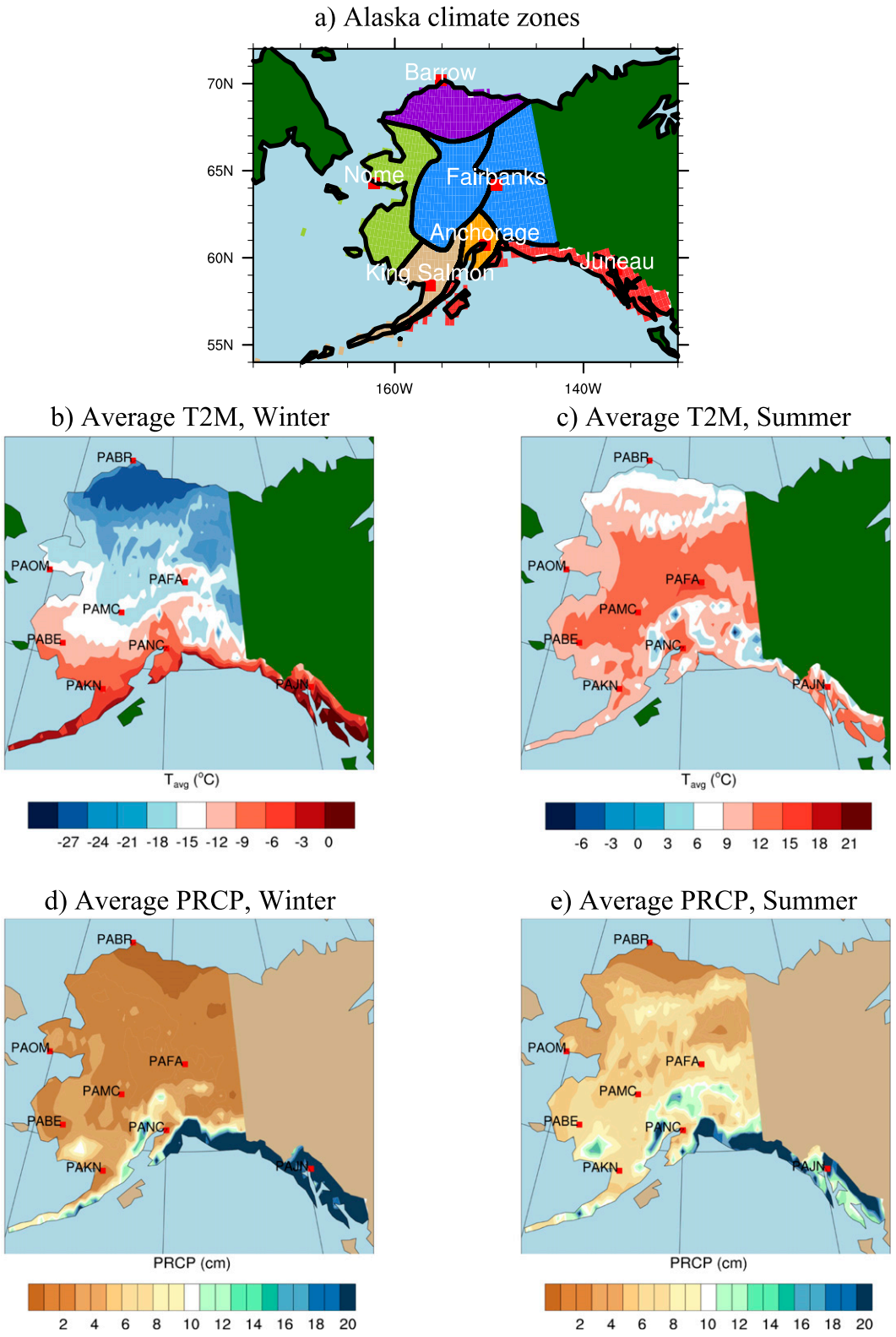

FIG. 1. (a) The Alaska climate zones in this study: Southeast (red), Cook Inlet (orange), Bristol Bay (brown), West Coast (light green), Interior (blue), and North Slope (purple). The 13 original divisions from Bieniek et al. (2012) are shown with black lines. Also pictured are seasonal climate averages from Hill et al. (2015) for (b) winter 2-m temperature, (c) summer 2-m temperature, (d) winter precipitation, and (e) summer precipitation.

follows (hereinafter the zones will be capitalized for easy recognition):

1) The ''Southeast'' zone is temperate and wet, with land cover/vegetation that includes expansive glaciers and coniferous forest. It is the warmest part of Alaska during winter, with average temperatures near freezing (Fig. 1b). Many locations in the Southeast zone receive more than 30 cm of precipitation per month during the winter (Fig. 1d), making this zone prone to flooding and landslides.
2) The ''Cook Inlet'' zone to the north and west is cooler and drier. It lies south of the Alaska Range, which isolates it from continental air to the north. With a mix of spruce and birch forest, wildfire is a natural hazard in the Cook Inlet zone during summer.
3) The ''Bristol Bay'' climate zone, which is a combination of low-lying river plains and alpine tundra, encompasses much of southwestern Alaska and extends through the Aleutians. The Bristol Bay zone is often subjected to severe storms exiting the North Pacific Ocean. Despite its maritime location, the Bristol Bay zone is much drier than the Southeast zone, with an average monthly summer precipitation near 9.0 cm (Fig. 1e).
4) The ''West Coast'' zone lies to the north of the Bristol Bay zone and is primarily low-lying shrub tundra. This zone is prone to severe river flooding during spring ice breakup and to coastal erosion, particularly in autumn when strong low pressure centers track across the Bering Sea. The sea ice edge extends southward and adjacent to the West Coast zone during winter, which causes it to exhibit both maritime and continental climate characteristics throughout the year.
5) The ''Interior'' zone is the largest and is bounded by the Alaska Range to the south and the Brooks Range to the north. The Interior, with its boreal forest, is both the hottest and coldest zone in terms of daily extremes, with temperatures that typically range from −50° to 35°C. The average surface temperature during summer, near 11.8°C, is the warmest of all zones (Fig. 1c). Wildfire, river flooding, and extreme cold highlight the weather found in the Interior zone.
6) The ''North Slope'' zone lies north of the Brooks Range and has tundra vegetation. It is the coldest and driest zone during all seasons. The North Slope includes the Arctic coast of Alaska, which is prone to coastal erosion, particularly during autumn when powerful storms bring ice-free water ashore.

2. Methods

Atmospheric reanalyses provide an estimate of the weather and climate that is valuable to stakeholders in the observation-sparse Arctic, but an understanding of the models is necessary to use these data effectively. Plots of observed (Fig. 2a) and reanalysis-model (Figs. 2b–f) terrain height show that higher-resolution models better represent the complex topography in Alaska, such as the Brooks Range and the Alaska Range. There are other potential issues occurring in or affecting the reanalyses, such as intrinsic model bias, observational quality, and the quality control of suspect observations. The impacts of these problems likely vary among the different reanalyses. The validation and reanalysis datasets are briefly described in this section.

a. Meteorological surface observations

Hill et al. (2015) developed a high-resolution (2 km) gridded dataset of monthly 2-m air temperature and precipitation that encompasses Alaska from 1961 to 2009 to serve the needs of the hydrometeorology community. A delta downscaling method (Hayhoe 2010) was applied to station data from 150 sites for temperature and 200 sites for precipitation to create the gridded fields. Temperature anomalies were calculated as the difference between station observations and climatological norms at that station, which were based on Parameter–Elevation Regressions on Independent Slopes Model (PRISM) data (Daly et al. 1994). These anomalies were interpolated onto the PRISM grid using a tension-with-splines method to develop an anomaly field. The anomaly field was then added to the PRISM climatological norms to produce the high-resolution gridded data for each month. For precipitation, Hill et al. (2015) computed proportional anomalies relative to the PRISM climatological norm to avoid negative values.

In this study, the reanalysis temperature [section 3a(1)] and precipitation [section 3a(2)] are compared with Hill et al. (2015) for 1979–2009. The reanalysis datasets and Hill et al. (2015) have been resampled to ½° latitude × ½° longitude spatial resolution for comparison. The reference climatological averages that are shown in Figs. 1b–e represent the resampled Hill et al. (2015) data. As in all observational datasets, the Hill et al. (2015) data have biases, but they serve as a baseline with which one can easily compare the different reanalyses.

Data obtained from the National Centers for Environmental Information Global Summary of Day (GSOD) product for six meteorological stations in Alaska are also used to validate the reanalyses in this study (section 3b). GSOD reports daily data in coordinated universal time from 0000 to 2359 UTC, which is temporally consistent with the reanalysis output. In contrast, the Global Historical Climatology Network (GHCN) station data are reported from local midnight to midnight. A notable difference was found when

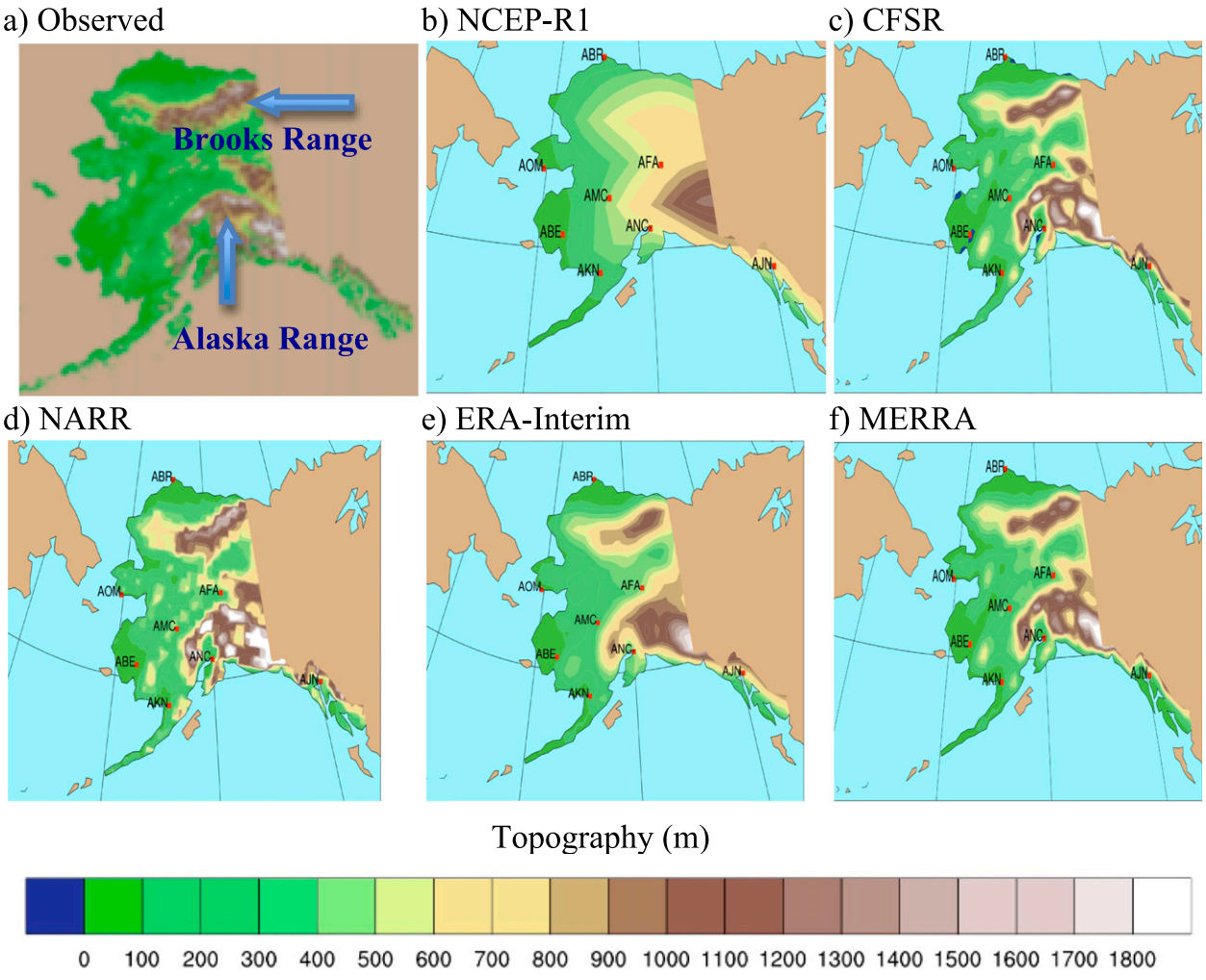

FIG. 2. Topography (a) observed (1 km) and for (b) R1 (210 km), (c) CFSR (38 km), (d) NARR (32 km), (e) ERA-Interim (79 km), and (f) MERRA (65 km). The numbers in parentheses here are the approximate spatial resolutions. The source of the Alaska digital elevation-model data is the U.S. Geological Survey. The latitudes and longitudes span 52°–72°N and 180°–210°E, respectively.

computing daily statistics with GSOD data as opposed to GHCN. For example, daily maximum temperatures, which typically occur near 0000 UTC in Alaska, are warmer in the GSOD data than in the GHCN data because extremely high values are essentially sampled twice in GSOD: once immediately before 0000 UTC and again shortly after. A comprehensive description of these data is available online (ftp://ftp.ncdc.noaa.gov/pub/data/gsod/readme.txt).

b. Reanalysis models

The R1 reanalysis uses a global spectral model with "T62" (210 km) horizontal resolution and 28 vertical sigma levels (Kalnay et al. 1996). Model output is available from 1948 to the present at up to 6-hourly temporal resolution. Three-dimensional variational data assimilation is performed using spectral statistical interpolation (Parrish and Derber 1992) to create the analyses. The 2-m temperature field is considered to be a class-B variable, which indicates that it is influenced directly by assimilated observations (satellite retrievals and radiosondes) and the atmospheric model. Observations of 2-m temperature are not assimilated, however. Kistler et al. (2001) note that R1 has a cold bias from a radiation imbalance that reflects too much shortwave radiation and allows too much longwave radiation to escape. Precipitation rate is a class-C variable, meaning it is strongly influenced by the model.

The NCEP NARR was developed to provide an accurate land hydrological dataset over North America (Mesinger et al. 2006). NARR uses the Eta Model and is coupled to the four-layer Noah land surface model (Ek et al. 2003). NARR has a spatial resolution of 32 km with 45 vertical levels and provides information from 1979 to the present at up to 3-hourly time intervals. Similar to

R1, NARR does not assimilate 2-m temperature observations. For Canada, rain gauge observations were assimilated prior to December of 2002, but the hydrologic fields are model derived thereafter. This observing system change induced a spurious climate shift in the precipitation record (Ruane 2010). For Alaska, and the adjacent ocean surfaces north of 42.5°N, no precipitation observations are assimilated. This results in a nonphysical precipitation discontinuity around 150°W due to assimilation blending. Model precipitation in NARR is generally too high, but gets lowered by data assimilation (Ruane 2010).

The NCEP Climate Forecast System Reanalysis (CFSR), released in 2010, uses the Global Forecast System atmospheric model with spectral "T362" (~38 km) horizontal resolution and 64 vertical levels (Saha et al. 2010). CFSR has interactive ocean, land, and sea ice models and produces globally gridded data from 1979 to the present. The 2-m temperature field in CFSR is derived primarily from satellite radiances and radiosonde information; no station observations of 2-m temperature are assimilated. The precipitation analysis is generated using a combination of the pentad dataset of the Climate Prediction Center (CPC) Merged Analysis of Precipitation (CMAP; Xie and Arkin 1997) and the CPC daily gauge analysis. For Alaska, the precipitation analysis is heavily dependent on the model's 6-hourly forecast field, which operates as a first guess. CFSR has been shown to have high precipitation values across the Arctic (Cullather and Bosilovich 2011; Lindsay et al. 2014).

The ERA-Interim from the European Centre for Medium-Range Weather Forecasts uses a spectral "T255" (79 km) forecast model that is composed of atmosphere, ocean, and land components and operates with 12-hourly analysis cycles, producing gridded data from 1979 to the present (Dee et al. 2011). ERA-Interim employs four-dimensional variational data assimilation, which takes into account an observation in time and three spatial dimensions before it gets assimilated and appropriate quality-control measures are conducted. The reanalyses generally estimate 2-m air temperature by interpolating between the surface and the lowest model level, except for ERA-Interim, which directly assimilates observations. Precipitation is a model-derived field that combines surface observations of temperature and humidity along with radiosonde data.

In 2008 the National Aeronautics and Space Administration released MERRA, which produces meteorological data from 1979 to the present (Bosilovich 2008; Rienecker et al. 2011). MERRA utilizes the Goddard Earth Observing System atmospheric model, version 5.2.0, and data assimilation system ("GEOS-5 DAS"). The spatial resolution is ½° latitude × ⅔° longitude (nominally 65 km) with 72 vertical levels, with up to hourly output. Neither 2-m temperature nor gauge precipitation is directly assimilated into MERRA, which enables the use of these surface observations for independent validation to assess the quality of the analyzed fields. MERRA assimilates instantaneous satellite data from the Special Sensor Microwave Imager (SSM/I) for rain-rate observations.

3. Comparison of reanalysis products with observed data

a. A regional evaluation of reanalyses for Alaska

This section presents gridded climate statistics of near-surface air temperature [section 3a(1)] and precipitation [section 3a(2)] from the five reanalyses for Alaska and quantifies these statistics over six regions that are based on climate zones. The spatial maps are constructed from monthly data that have been seasonally averaged and are presented for winter (November–March) and summer (June–August). Each set of six maps contains an ensemble of all reanalysis-model differences, as well as each reanalysis's model difference relative to the reference climatological average for winter temperature (Figs. 3a–f), summer temperature (Figs. 3g–l), winter precipitation (Figs. 4a–f), and summer precipitation (Figs. 4g–l). Tabular values aggregated over six climate zones for mean, bias, and standard deviation for the 31-yr period are presented for temperature (Table 1) and precipitation (Table 2).

1) NEAR-SURFACE AIR TEMPERATURES

NARR has the smallest winter temperature bias across the West Coast, Interior, Bristol Bay, and Cook Inlet climate zones and the largest winter bias for the North Slope (+1.8°C). All of the reanalyses have a winter cold bias in the Interior and Cook Inlet climate zones. The statewide ensemble bias during winter (2.29°C; Fig. 3a) is smaller than that of any individual reanalysis, with NARR having the next-smallest bias (2.32°C; Fig. 3d).

In summer, ERA-Interim has the smallest temperature bias (Fig. 3k) in the West Coast, Interior, and Southeast climate zones. The R1 has a cold bias across Alaska (Fig. 3h), which is most pronounced in the Interior (−2.9°C), and Cook Inlet (−2.3°C) zones. The statewide ensemble bias (1.61°C; Fig. 3g) is smaller than that of any individual reanalysis, with CFSR having the next-lowest bias (1.64°C; Fig. 3i).

Observed near-surface temperature variability (standard deviation) is climatologically largest during the winter season and lowest in summer (Table 1). This is

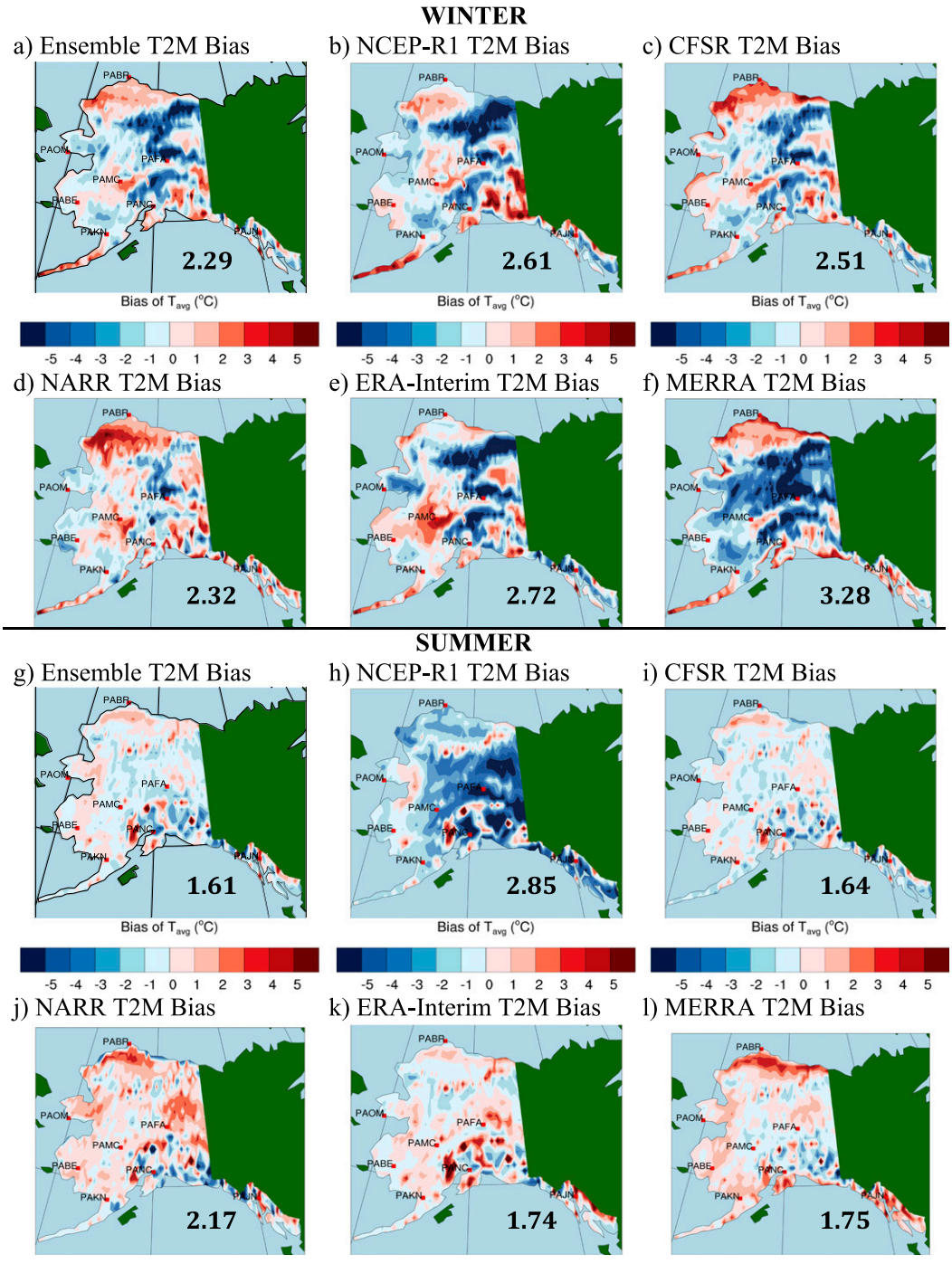

FIG. 3. Two-meter temperature in (a)–(f) winter (November–March) and (g)–(l) summer (June–August), 1979–2009. Ensemble mean of the reanalyses is in (a) and (g), followed by model bias in (b)–(f) and (h)–(l), defined as observed minus reanalysis. RMS differences (°C) are indicated in boldface type in each panel. The latitudes and longitudes span 52°–72°N and 180°–210°E, respectively.

reflected by the larger bias magnitudes for surface temperature during winter. CFSR and MERRA routinely have the closest statewide representation of winter temperature variability relative to the Hill et al. (2015) dataset. During winter, the models overestimate the variability for the West Coast and North Slope, underestimate it in southern Alaska, and generally match the observed variability in Interior Alaska (Table 1). In

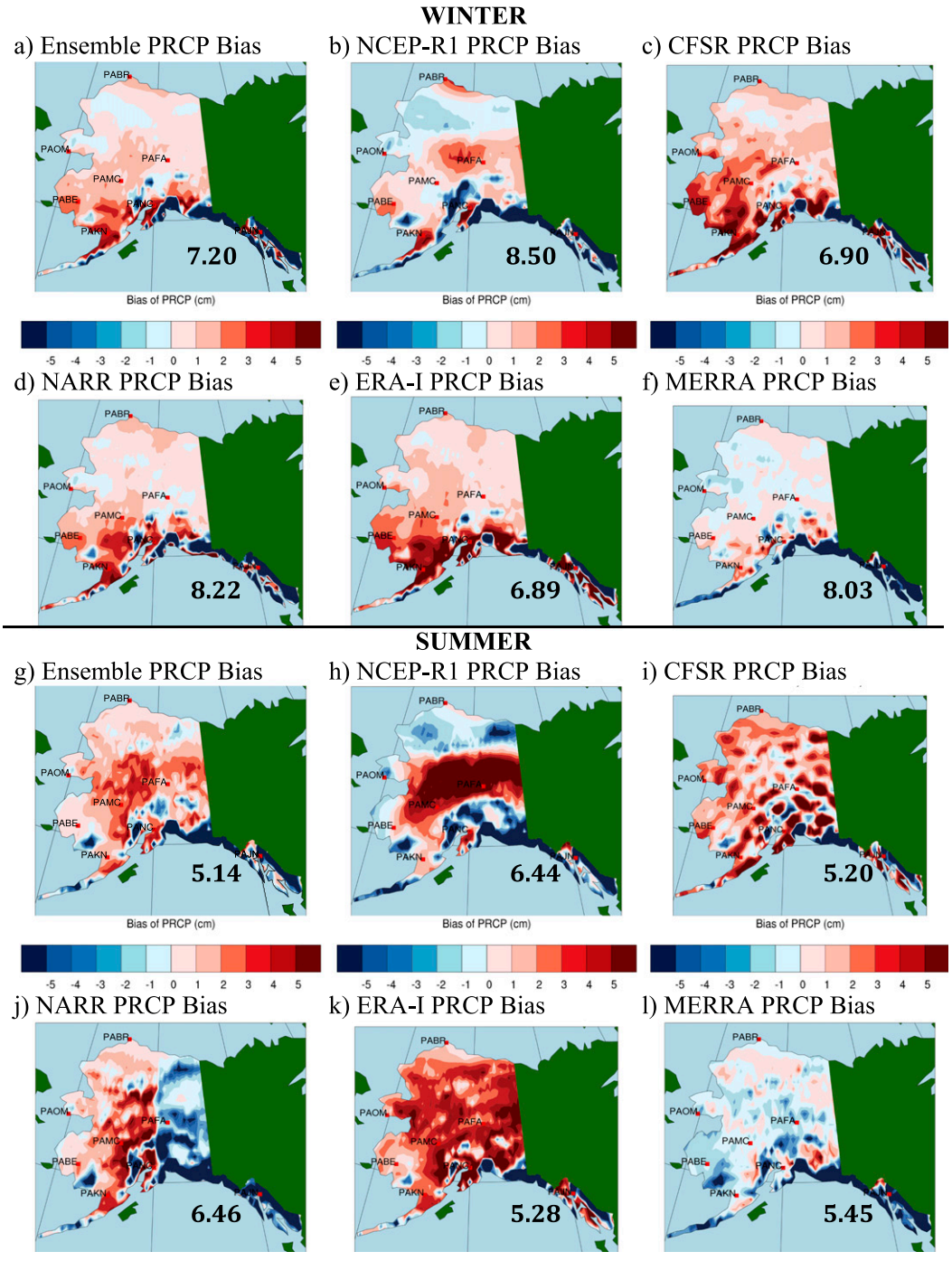

FIG. 4. As in Fig. 3, but for precipitation.

summer, ERA-Interim has the best representation of temperature variability for all climate zones, but all reanalyses overestimate summer temperature variability (Table 1).

2) PRECIPITATION

The reanalyses are generally too wet across northern Alaska, and they are too dry in the Southeast during winter. Both ERA-Interim (Fig. 4e) and CFSR (Fig. 4c) show a smaller bias individually than the statewide ensemble mean (Fig. 4a). The R1 (Fig. 4b) and MERRA (Fig. 4f) have negative winter precipitation biases in the Southeast of −14.0 and −13.9 cm month^{-1}, respectively. This result suggests that the reanalyses are predicting about 50% of the observed precipitation in the Southeast,

TABLE 1. Seasonally averaged monthly average temperature (TAVG; °C) by climate zone, bias (°C) relative to the Hill et al. (2015) data, and standard deviation (°C).

	Winter			Summer		
	TAVG	Bias	Std dev	TAVG	Bias	Std dev
North Slope						
R1	−24.3	−0.9	4.1	6.5	−1.3	1.7
CFSR	−22.4	1.0	3.8	7.8	0.0	1.9
NARR	−21.6	1.8	3.5	8.5	0.7	1.9
ERA	−24.7	−1.3	4.1	8.0	0.2	1.5
MERRA	−22.6	0.8	3.5	9.3	1.5	1.7
Hill et al. (2015)	−23.4	—	3.5	7.8	—	1.3
West Coast						
R1	−14.8	−0.8	4.2	10.1	−0.8	1.4
CFSR	−13.7	0.3	3.7	10.6	−0.3	1.6
NARR	−14.3	−0.3	4.1	11.4	0.5	1.5
ERA	−14.3	−0.3	4.2	10.8	−0.1	1.4
MERRA	−15.0	−1.0	3.6	11.5	0.6	1.4
Hill et al. (2015)	−14.0	—	3.8	10.9	—	1.2
Interior						
R1	−17.4	−1.0	4.1	8.9	−2.9	1.9
CFSR	−17.4	−1.0	3.9	11.4	−0.4	1.6
NARR	−16.5	−0.1	3.7	12.3	0.5	1.6
ERA	−17.5	−1.1	4.1	12.0	0.2	1.3
MERRA	−19.4	−3.0	3.9	11.6	−0.2	1.4
Hill et al. (2015)	−16.4	—	3.9	11.8	—	1.2
Bristol Bay						
R1	−5.9	0.1	3.0	9.6	−0.9	1.2
CFSR	−6.3	−0.3	3.3	10.3	−0.2	1.1
NARR	−6.1	−0.1	3.3	10.5	0.0	1.0
ERA	−5.6	0.4	3.3	11.0	0.5	0.9
MERRA	−6.7	−0.7	3.3	11.2	0.7	1.1
Hill et al. (2015)	−6.0	—	3.5	10.5	—	0.9
Cook Inlet						
R1	−9.0	−1.1	3.1	8.0	−1.9	1.7
CFSR	−9.0	−1.1	2.9	9.6	−0.3	1.4
NARR	−8.6	−0.7	2.9	9.1	−0.8	1.4
ERA	−9.3	−1.4	3.5	10.9	1.0	1.1
MERRA	−9.2	−1.3	3.2	10.5	0.6	1.2
Hill et al. (2015)	−7.9	—	3.4	9.9	—	1.1
Southeast						
R1	−2.5	0.1	2.2	8.4	−2.3	1.3
CFSR	−3.0	−0.4	2.5	9.7	−1.0	1.1
NARR	−2.2	0.4	2.2	9.7	−1.0	1.1
ERA	−3.0	−0.4	2.6	10.6	−0.1	1.0
MERRA	−1.7	0.9	2.3	11.7	1.0	1.1
Hill et al. (2015)	−2.6	—	2.5	10.7	—	1.0

TABLE 2. Seasonally averaged monthly average precipitation (MPRCP; cm) by climate zone, bias (cm) relative to the Hill et al. (2015) data, and standard deviation (cm).

	Winter			Summer		
	MPRCP	Bias	Std dev	MPRCP	Bias	Std dev
North Slope						
R1	1.0	−0.3	0.7	2.6	−1.5	1.3
CFSR	2.0	0.7	1.0	6.1	2.0	2.6
NARR	2.0	0.7	0.9	4.2	0.1	2.0
ERA	1.9	0.6	1.0	6.4	2.3	2.1
MERRA	1.2	−0.1	0.6	4.0	−0.1	1.5
Hill et al. (2015)	1.3	—	0.8	4.1	—	2.0
West Coast						
R1	2.9	0.0	1.7	5.7	0.2	2.2
CFSR	5.0	2.1	2.4	7.4	1.9	3.1
NARR	3.8	0.9	2.0	6.2	0.7	2.6
ERA	4.5	1.6	2.4	7.9	2.4	2.9
MERRA	2.7	−0.2	1.5	4.5	−1.0	1.8
Hill et al. (2015)	2.9	—	1.9	5.5	—	2.4
Interior						
R1	3.0	0.4	1.5	9.6	2.8	2.8
CFSR	3.8	1.2	2.0	8.6	1.8	3.6
NARR	3.0	0.4	1.6	6.2	−0.6	2.8
ERA	3.7	1.1	1.9	10.1	3.3	3.1
MERRA	2.5	−0.1	1.3	6.0	−0.8	2.1
Hill et al. (2015)	2.6	—	1.9	6.8	—	3.1
Bristol Bay						
R1	6.1	−0.7	2.7	7.3	−1.7	2.4
CFSR	10.1	3.3	3.9	10.5	1.5	3.4
NARR	8.3	1.5	3.3	8.8	−0.2	2.9
ERA	10.3	3.5	4.1	10.6	1.6	3.5
MERRA	6.1	−0.7	2.6	6.8	−2.2	2.2
Hill et al. (2015)	6.8	—	3.7	9.0	—	4.0
Cook Inlet						
R1	6.5	−3.9	3.2	7.8	−3.3	2.7
CFSR	11.0	0.6	5.3	12.4	1.3	4.5
NARR	10.0	−0.4	5.1	9.5	−1.6	4.3
ERA	12.9	2.5	6.2	13.3	2.2	4.5
MERRA	8.8	−1.6	4.4	8.8	−2.3	3.4
Hill et al. (2015)	10.4	—	7.4	11.1	—	6.3
Southeast						
R1	15.5	−14.0	5.6	9.7	−8.6	3.8
CFSR	25.5	−4.0	10.0	16.0	−2.3	6.2
NARR	20.8	−8.7	8.7	8.9	−9.4	4.7
ERA	25.9	−3.6	10.1	14.4	−3.9	6.0
MERRA	15.6	−13.9	6.2	9.2	−9.1	4.0
Hill et al. (2015)	29.5	—	14.0	18.3	—	8.5

and this bias is likely due to smoothed topography in the models. MERRA has the smallest winter precipitation bias (Fig. 4f) for the North Slope, Interior, and Bristol Bay climate zones.

The reanalyses display different patterns during summer, but, similar to winter, they all show large negative precipitation biases in the Southeast. CFSR has the smallest bias of $-2.3\,\mathrm{cm\,month^{-1}}$ in the Southeast (Table 2), and this accounts for its relatively small statewide bias (Fig. 4i). NARR has the smallest precipitation bias (Fig. 4j) across the North Slope, Interior, and Bristol Bay climate zones but shows an unrealistic meridional boundary around 150°W that is due to assimilation blending, as noted earlier, with too much precipitation to the west of this line and too little to its east (Ruane 2010). The R1 has a notable wet bias across the Interior during summer, with monthly anomalies greater than 5 cm locally (Fig. 4h). ERA-Interim is too wet throughout most of the state and too dry in parts of

south-coastal Alaska (Fig. 4k). MERRA shows large dry biases across the Southeast (Fig. 4l).

The highest precipitation variability for most of Alaska occurs during summer, although for regions south of the Alaska Range the peak is either in autumn or winter. The standard deviation of monthly precipitation in Hill et al. (2015) during summer varies from 2.0 cm for the North Slope up to 8.5 cm for the Southeast (Table 2). In winter, the contrast is greater, when the standard deviation for the North Slope decreases to 0.8 cm but the Southeast increases to 14.0 cm. ERA-Interim most closely represents observed precipitation variability in summer and winter. The reanalyses all underestimate precipitation variability for the Cook Inlet and Southeast climate zones, which is likely due to an inadequate representation of terrain in their underlying models.

b. *A station-based evaluation of reanalyses for Alaska*

This section presents 31-yr averaged time series of observed daily maximum temperature T_{max} (Figs. 5a–f), minimum temperature T_{min} (Figs. 6a–f), and precipitation PRCP (Figs. 7a–f) for six Alaskan stations. This analysis highlights consistencies between the monthly reanalysis data, which were analyzed spatially, and the daily station data. The seasonal cycle of reanalysis-model bias relative to these observations is included and represents data from the land grid cell that is nearest to each station. There is one station per climate zone in this study—Barrow (North Slope), Fairbanks (Interior), Juneau (Southeast), King Salmon (Bristol Bay), Anchorage (Cook Inlet), and Nome (West Coast).

Fairbanks (Interior) has the largest annual range of near-surface air temperature: the climatological mean T_{max} in January and July differs by 40°C (Fig. 5b). Juneau displays the least variability and has an annual range of ~20°C (Fig. 5c). The reanalyses show temperature biases between −5° and +5°C, with a tendency toward cool biases for daily T_{max} (Fig. 5) and warm biases for T_{min} (Fig. 6). The exceptions are positive T_{max} biases at Barrow during summer (Fig. 5a) and negative T_{min} biases at Juneau (Fig. 6c) and Anchorage (Fig. 6e). The R1 is the coldest reanalysis for Fairbanks (Fig. 5b) and Anchorage (Fig. 5e), with T_{max} biases that exceed 10°C during summer. ERA-Interim, considered to be the top-performing reanalysis with respect to summer temperature bias in the Interior, also shows persistent cold biases of 5°C during the summer months at Fairbanks and Anchorage. These findings likely reflect local topographical effects where the nearest model gridcell elevation is too high relative to the station.

Mean daily precipitation varies from near zero at Barrow for much of the year (Fig. 7a) to greater than 10 mm day^{-1} at Juneau in autumn (Fig. 7c). For locations north of the Alaska Range, peak precipitation falls in mid- to late summer, and for south-coastal Alaska the wettest period is during autumn. The reanalyses overestimate daily precipitation by 1–2 mm across Alaska, except at Juneau, where these biases often exceed 5 mm day^{-1}. This result contradicts the spatial precipitation analysis for the Southeast climate zone, which showed that the reanalyses were too dry. This contradiction occurs because Juneau's grid cell has too high of an elevation in the reanalyses. The R1 has large positive precipitation biases during summer at Fairbanks (Fig. 7b), often exceeding 4 mm day^{-1}, because of its cold bias. An excess amount of moisture is forced to condense and precipitate out in a colder atmosphere with each analysis cycle. CFSR shows the largest positive precipitation biases for Barrow (Fig. 7a), Juneau (Fig. 7c), and Nome (Fig. 7f).

c. *Station-based climate-extreme statistics*

This section presents climate-extreme indices averaged by decade for Barrow, Fairbanks, Juneau, and Nome. These include annual counts of extreme warm days (Fig. 8), extreme cold days (Fig. 9), extreme precipitation days (Fig. 10), and growing season length (Fig. 11). These indices are analogous to those from the Datasets for Indices of Climate Extremes (CLIMDEX) project (Karl et al. 1999; http://www.climdex.org/index.html), but the thresholds for these indices have been adjusted to be applicable to the Alaska climate, which is characterized by strong gradients of temperature and precipitation. For the temperature and precipitation indices, the thresholds used to count a daily extreme value approximately correspond to the 95th percentile of all observed daily values for each station. Growing-season length measures the number of days each year between the fifth consecutive day on which daily average temperature $T_{avg} > 0$°C and the day on which $T_{min} \leq -2.2$°C for each station.

Observed extreme-warm days (EWD; gray bars of Fig. 8) at Barrow ($T_{max} \geq 15$°C; Fig. 8a), Fairbanks ($T_{max} \geq 25$°C; Fig. 8b), and Nome ($T_{max} \geq 20$°C; Fig. 8d) do not display a significant trend over 1979–2009, whereas in Juneau ($T_{max} \geq 25$°C; Fig. 8c) the number of EWD has approximately doubled between the 1980s and 2000s. The reanalysis counts of annual EWD are highly variable but generally overestimate the count in Barrow while underestimating the count in Nome, Fairbanks, and Juneau. The R1 and ERA-Interim produce few, if any, EWD at Fairbanks. This is consistent with these models having a cold bias during summer, likely because of the higher elevation of the Fairbanks grid cell relative to the station.

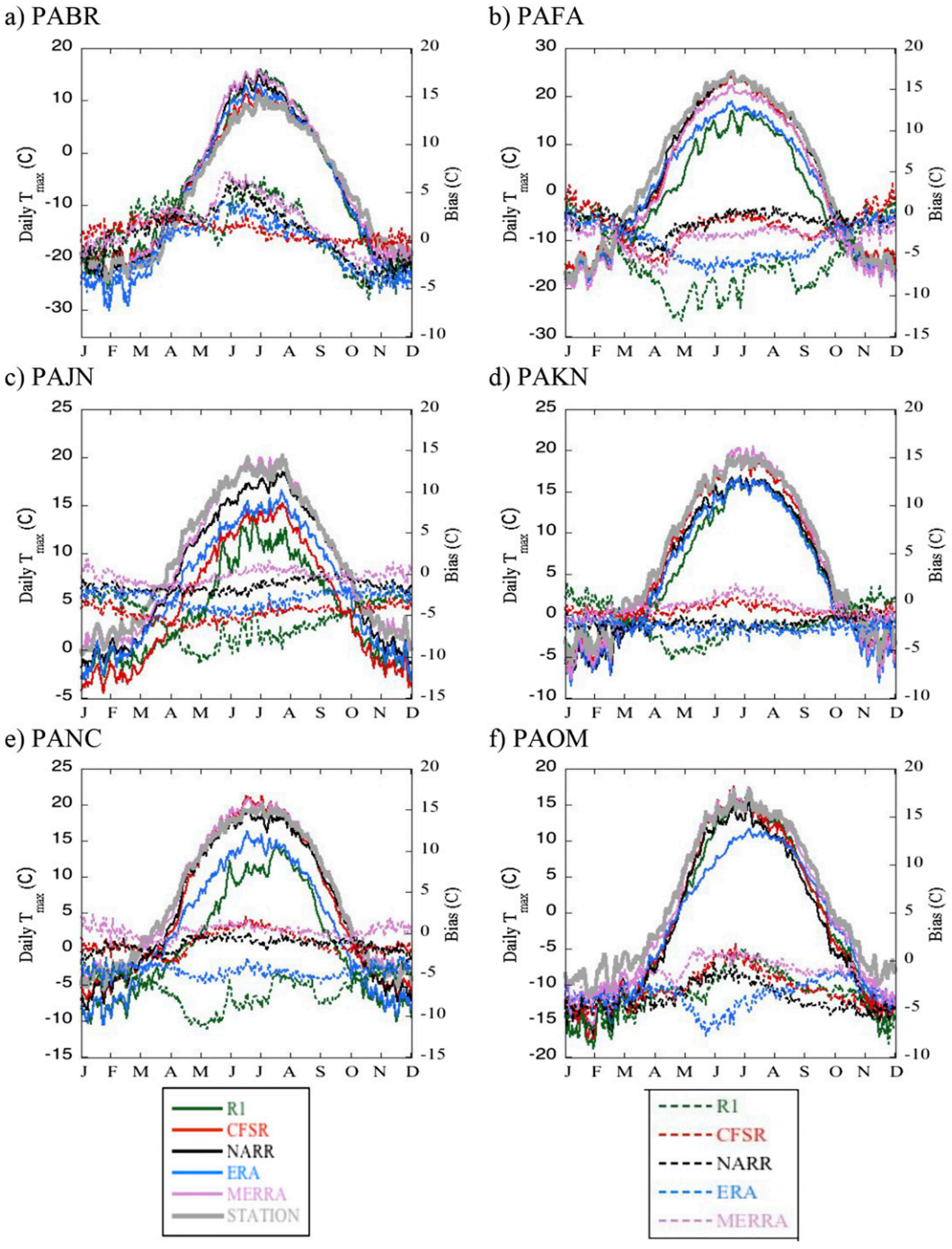

FIG. 5. Daily T_{max} (°C; solid lines) and bias of T_{max} (°C; dashed lines) at (a) Barrow, (b) Fairbanks, (c) Juneau, (d) King Salmon, (e) Anchorage, and (f) Nome. The reanalyses are compared with station observations (gray), 1979–2009.

The observed extreme-cold days (ECD; gray bars of Fig. 9) count at Barrow ($T_{min} \leq -40$°C; Fig. 9a) is declining, which is consistent with a warming trend at Barrow of 0.52°C $(10\,yr)^{-1}$ since 1977 (Hartmann and Wendler 2005). Fairbanks ($T_{min} \leq -40$°C; Fig. 9b), Juneau (Fig. 9c), and Nome ($T_{min} \leq -30$°C; Fig. 9d) do not display an observed trend of ECD. At Barrow, ERA-interim and R1 overestimate the ECD count by more than 100% while the other models underestimate the count. At Nome, R1 and CFSR overestimate the

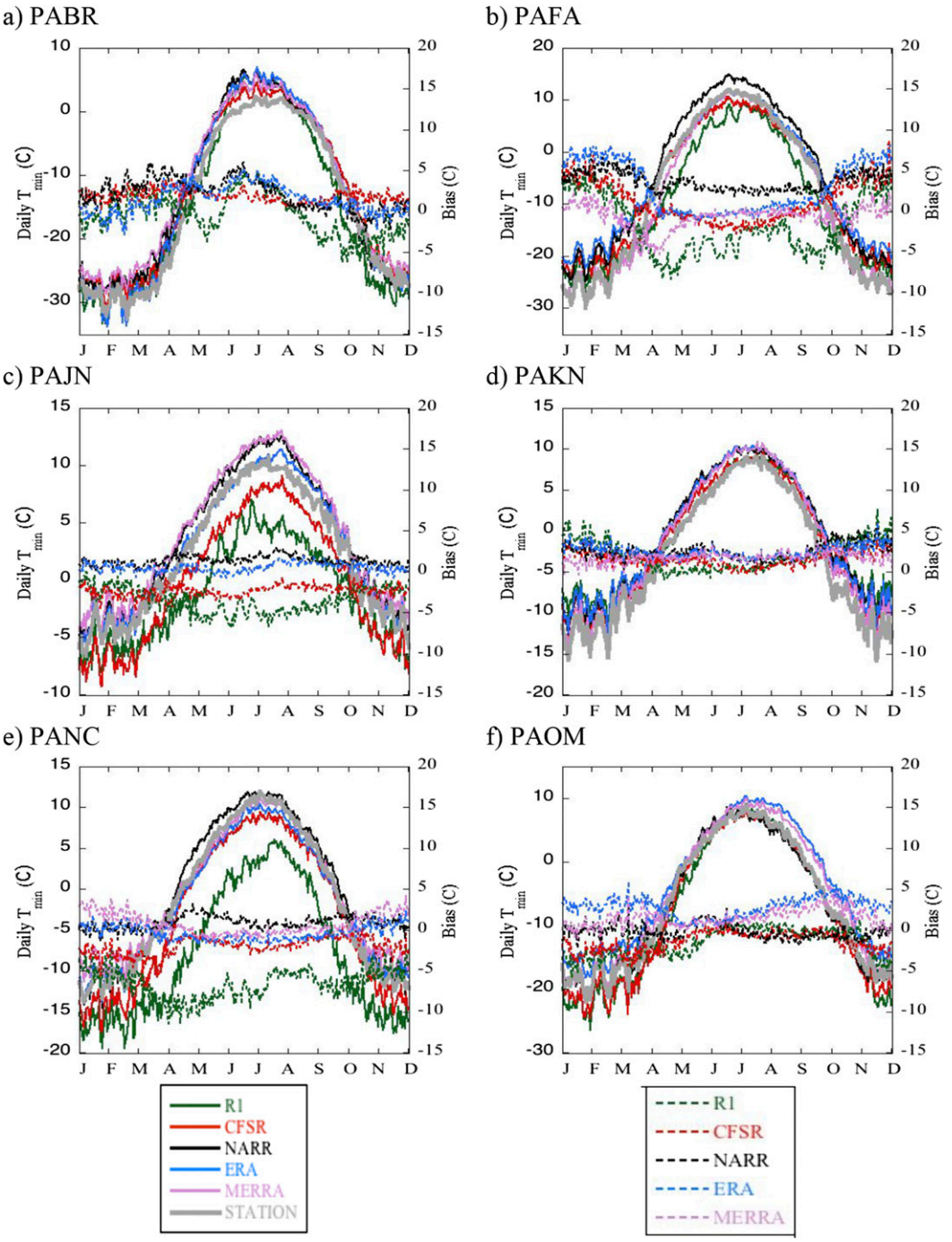

FIG. 6. As in Fig. 5, but for T_{min}.

count and ERA-Interim and MERRA underestimate the count. At Fairbanks, MERRA is the only reanalysis that closely represents the number of ECD ($T_{min} \leq -40°C$), which suggests that MERRA represents low-level inversions better than the other models. In Juneau (Fig. 9c), R1 and CFSR overestimate the ECD count.

Observed extreme-precipitation days (EPD; gray bars of Fig. 10) at Barrow (PRCP $\geq$ 5 mm; Fig. 10a), Fairbanks (PRCP $\geq$ 10 mm; Fig. 10b), Juneau (PRCP $\geq$ 25 mm; Fig. 10c), and Nome (PRCP $\geq$ 10 mm; Fig. 10d) do not display a notable trend from 1979 to 2009. The reanalyses generally overestimate EPD at Barrow, except for R1 (underestimated) and MERRA (close to

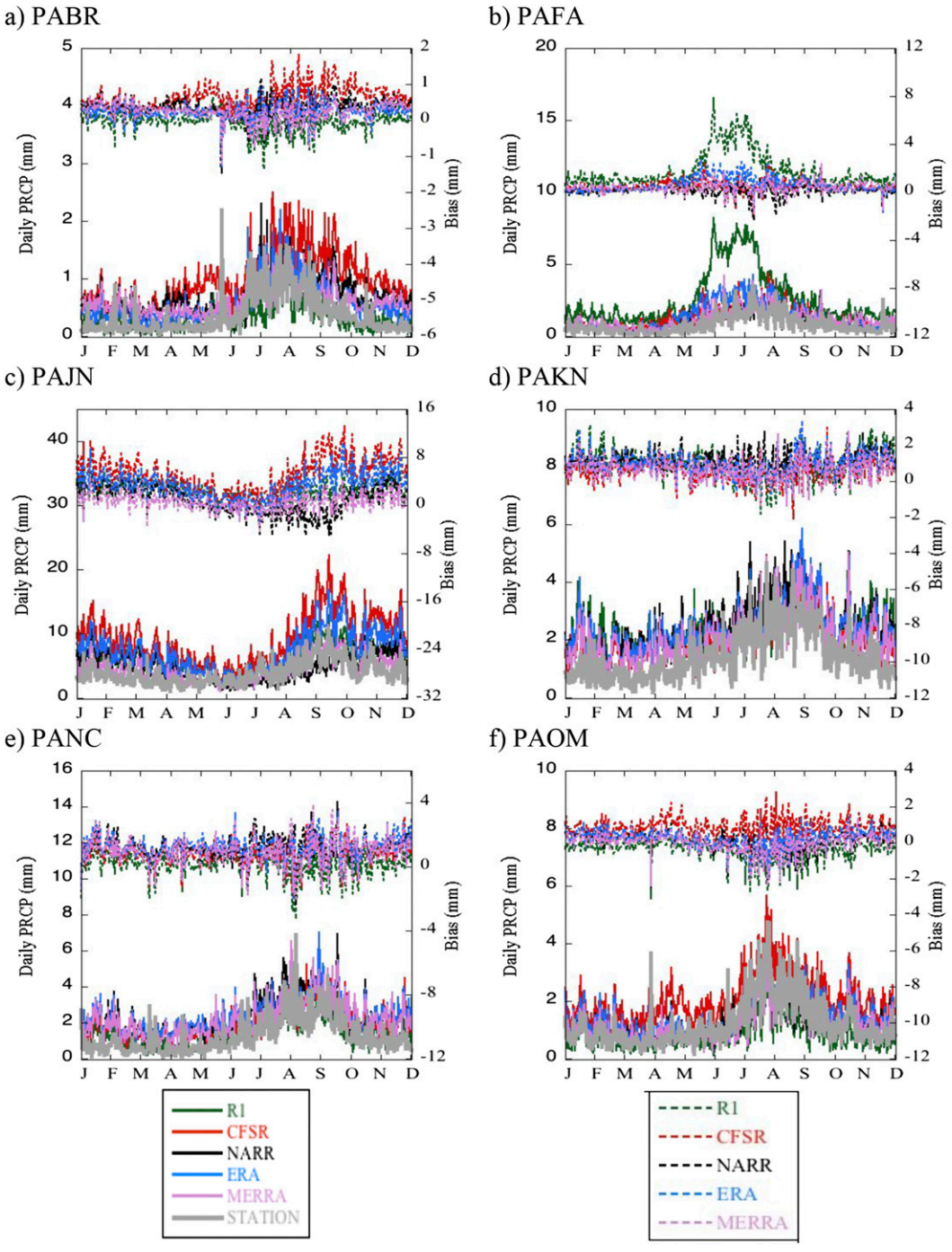

FIG. 7. As in Fig. 5, but for PRCP (mm). All PRCP values represent the 31-yr mean for each day.

observed). CFSR displays larger-than-observed counts of EPD at Nome while R1 is lower than observed. For Fairbanks, R1 has more than 2 times the number of observed EPD, which is consistent with its wet bias during summer. NARR underestimates heavy precipitation at Fairbanks prior to the 2000s before there is a dramatic uptick, which is due to the change in data assimilation across Canada and the oceans adjacent to Alaska. Juneau EPD counts from the reanalyses are generally close to observed, except for CFSR and ERA-Interim, which are much higher. The tendency for CFSR to overestimate mean precipitation carries over to daily

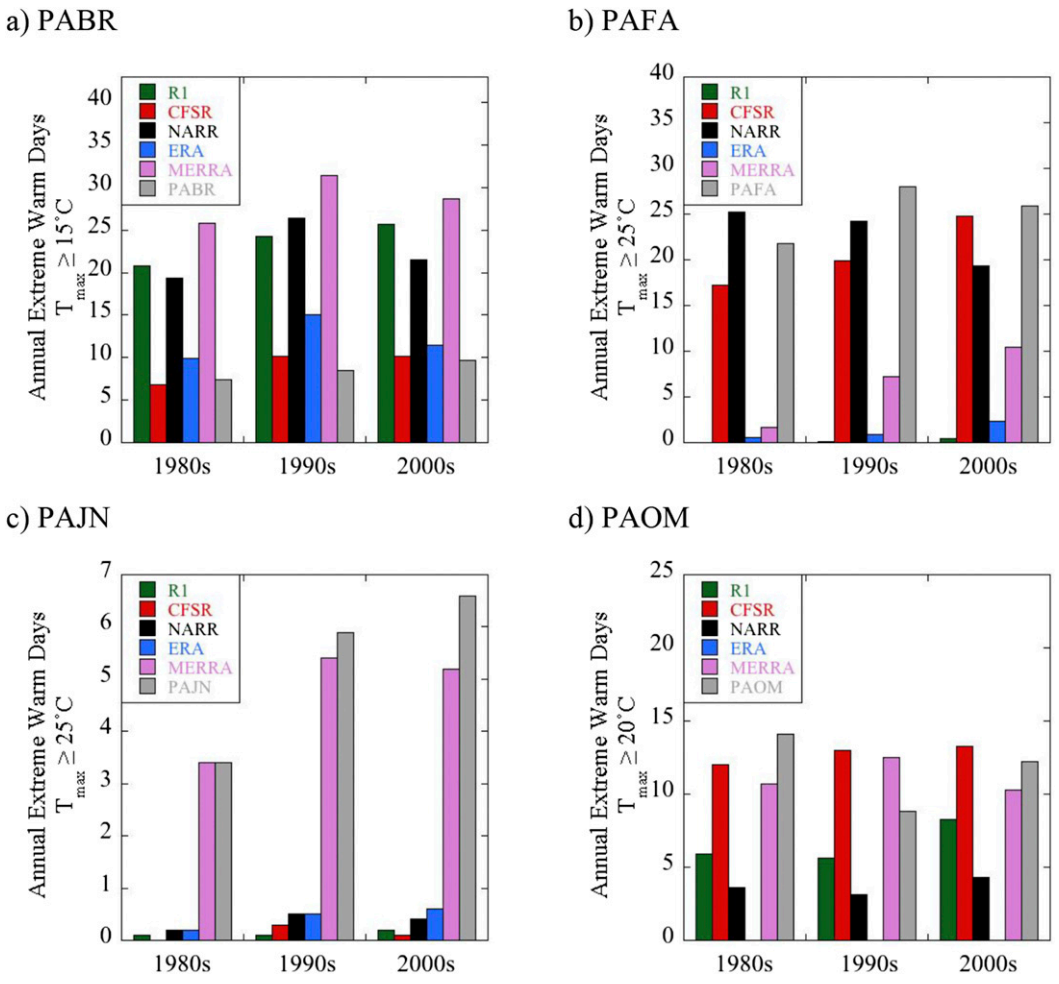

FIG. 8. Decadal-average annual counts of EWD at (a) Barrow ($T_{max} \geq 15°C$), (b) Fairbanks ($T_{max} \geq 25°C$), (c) Juneau ($T_{max} \geq 25°C$), and (d) Nome ($T_{max} \geq 20°C$).

extremes for which the number of CFSR EPD at all four stations is often 2 times the observed number.

Observed growing-season length (GSL) does not display any notable trends (gray bars of Fig. 11). Across Alaska, this index ranges from just over 40 days yr^{-1} at Barrow (Fig. 11a) up to 175 days yr^{-1} at Juneau (Fig. 11c). All of the reanalyses except R1 overestimate this index at Barrow by up to a factor of 2. The Nome (Fig. 11d) GSL for R1, NARR, and CFSR is close to observed and is about 20%–30% higher in ERA-Interim and MERRA. The R1 underestimates the GSL in Fairbanks (Fig. 11b) while the other models are close to observed. In Juneau, CFSR GSL is close to observed while NARR, ERA-Interim, and MERRA are longer than observed and R1 is too short, particularly in the first two decades. In general, the reanalysis models overestimate the length of the growing season, with the exception of R1, which routinely underestimates it for Fairbanks and Juneau.

4. Linkages between station and spatial data

Given the full spatial coverage of reanalysis data, they can provide climate information for remote locations in Alaska. Because of a dearth of station observations, however, it is not possible to evaluate the reanalysis data at each location at which climate information is needed. To address this issue, we constructed one-point correlations between station observations and gridded data to identify regions that have climate variability that is similar to that of a first-order meteorological station.

Winter (December–February) and summer (June–August) near-surface air temperature and precipitation correlations for R1, ERA-Interim, and Hill et al. (2015) are presented for Barrow, Fairbanks, Nome, King Salmon, Anchorage, and Juneau (Figs. 12–14). The correlation between the station data and the nearest grid point measures how well the reanalysis captures the seasonal variability and is shown by the number in each

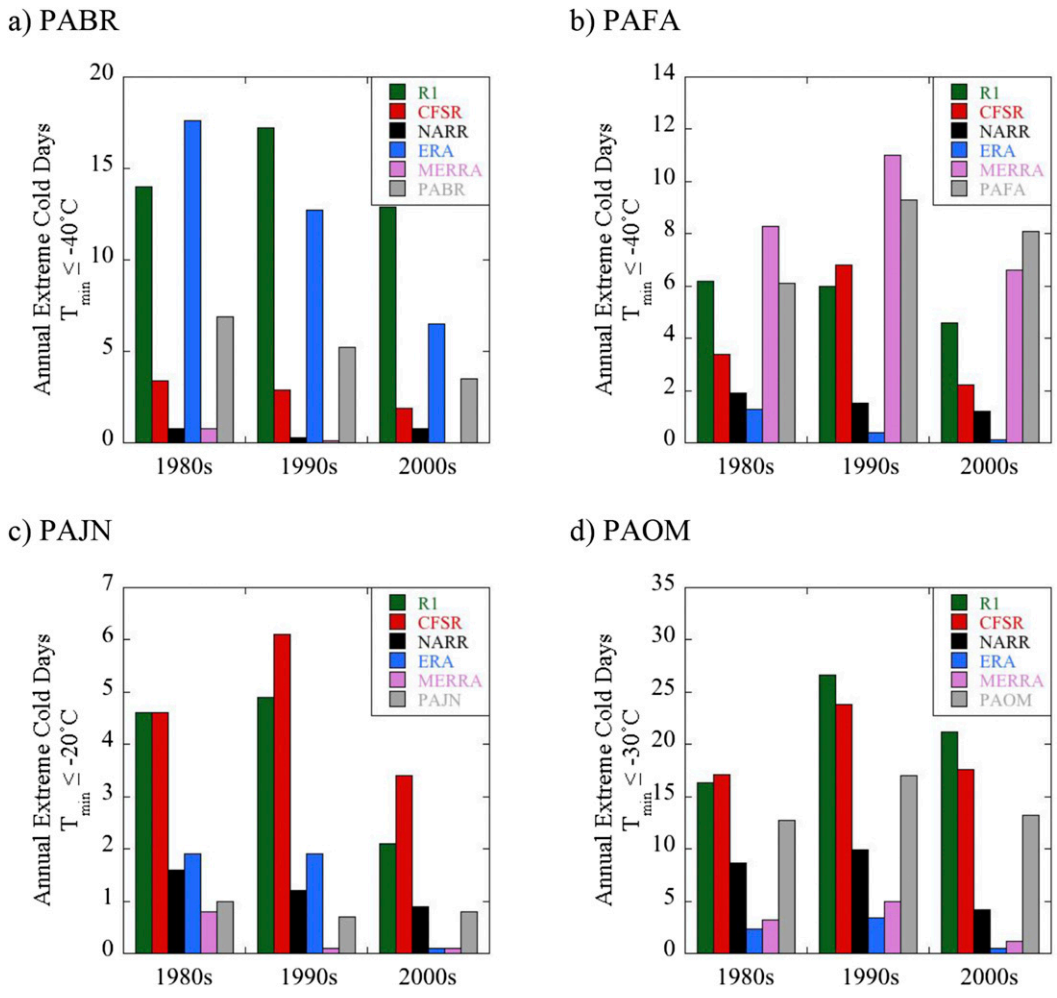

FIG. 9. Decadal-average annual counts of ECD at (a) Barrow ($T_{min} \leq -40°C$), (b) Fairbanks ($T_{min} \leq -40°C$), (c) Juneau ($T_{min} \leq -20°C$), and (d) Nome ($T_{min} \leq -30°C$).

panel. CFSR, NARR, and MERRA show correlation patterns that are similar to those of ERA-Interim and are therefore not shown.

The reanalysis and Hill et al. (2015) time series for the correlations originate from monthly data that have been averaged seasonally. The daily station data contain observations of T_{max} and T_{min}, which are averaged to compute daily mean temperature. The daily data are then averaged into monthly and then seasonal values. The seasonal cycle is removed from all of the time series by using a mean calculated over the 1979–2009 period, and the correlations cover the 31-yr reference period. The point correlations in Figs. 12–14 are overlain by the climate-division lines (Bieniek et al. 2012), which identify boundaries between areas with similar climate variability.

Overall, winter and summer temperatures display large correlations between the station and nearest gridpoint values (see the numbers in Figs. 12–14). Winter temperatures have a slightly larger spatial scale than those of summer for the point correlations. During winter, ERA-Interim and R1 perform comparably well, but ERA-Interim performs better during summer.

Temperature correlations for Barrow and Nome display a seasonality that depends on sea ice. In winter Barrow is more closely associated with the Arctic Ocean and Bering Sea, whereas in the summer the correlations are higher over terrestrial North America. Likewise, for Nome much of the Bering Sea becomes ice covered and the climate across the West Coast is more continental in winter. For the Interior zone and Fairbanks, correlations are higher in winter because the reanalyses are able to predict the synoptic-scale height pattern, which is a better indicator of temperature during winter. The superior performance of ERA-Interim over R1 stands out during summer for Anchorage and Juneau. The R1

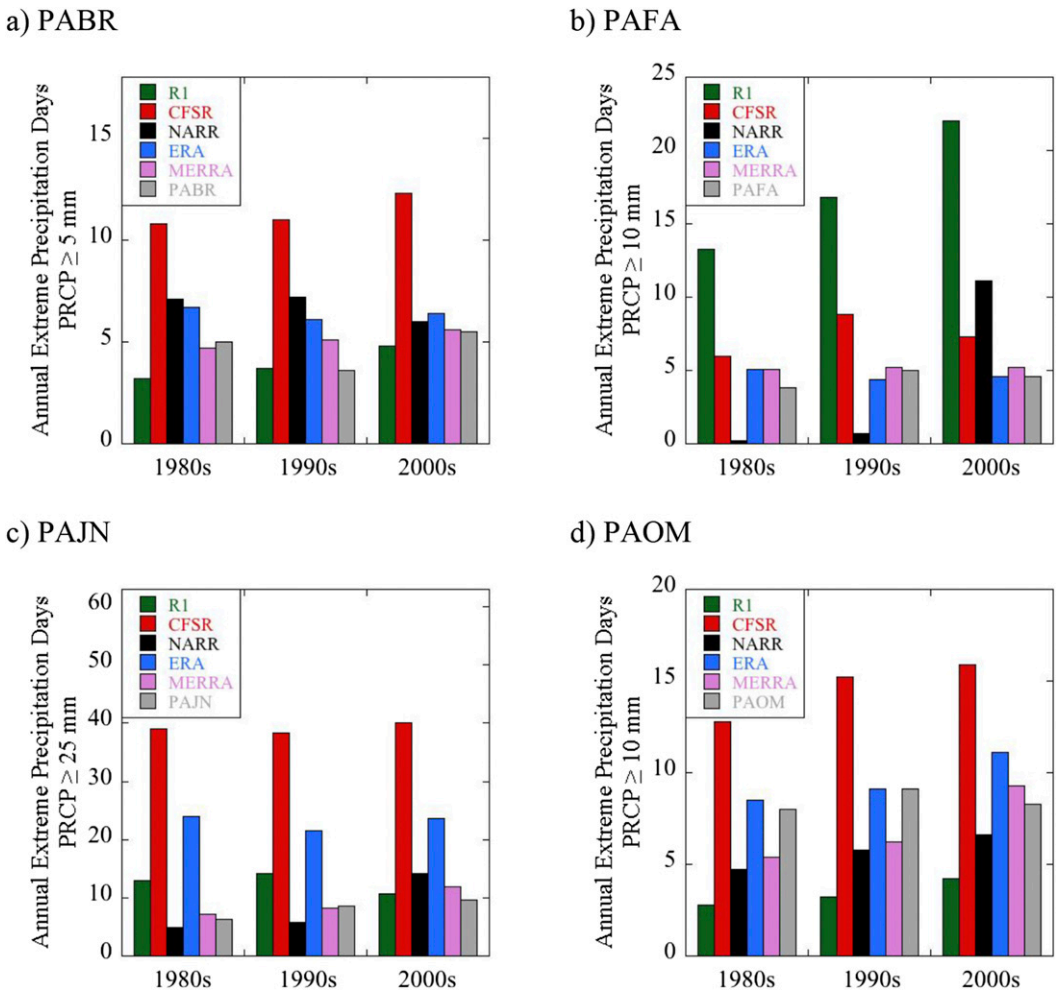

FIG. 10. Decadal-average annual counts of EPD at (a) Barrow (PRCP ≥ 5 mm), (b) Fairbanks (PRCP ≥ 10 mm), (c) Juneau (PRCP ≥ 25 mm), and (d) Nome (PRCP ≥ 10 mm).

displays very low temperature correlations at Anchorage (0.48; Fig. 14a) and Juneau (0.19; Fig. 14c), likely as a result of coarse model topography and high terrain gradients in these locations.

Winter and summer precipitation correlations are less than 0.8 between the station and the nearest gridpoint values, which is considerably less than the temperature correlations at most times. Winter point correlations for precipitation display a larger spatial scale than those of summer, and ERA-Interim performs better overall than R1 throughout Alaska except at Barrow. During winter Barrow precipitation is correlated with precipitation in Chukotka and the Bering Sea, whereas during summer the correlations are largest in the Chukchi and Beaufort Seas. In the Interior, winter precipitation correlations indicate a larger area of similar variability than during summer. This result is consistent with synoptic forcing for winter precipitation but more convective, localized precipitation during summer.

5. Synthesis and conclusions

By now it is evident that the choice of a "best" reanalysis depends on variable, season, and metric of evaluation. An ensemble approach tends to reduce statewide temperature bias, but not necessarily for precipitation. If we instead study the most impactful natural hazards that occur in Alaska and determine the reanalyses that most accurately predict the important meteorological variables surrounding these hazards rather than attempt to proclaim that one model fits all, then a few reanalyses stand out (Table 3).

Wildfire in Alaska has the capacity to burn millions of acres in a matter of a few weeks, primarily in the Interior and Cook Inlet zones. Such fires have direct

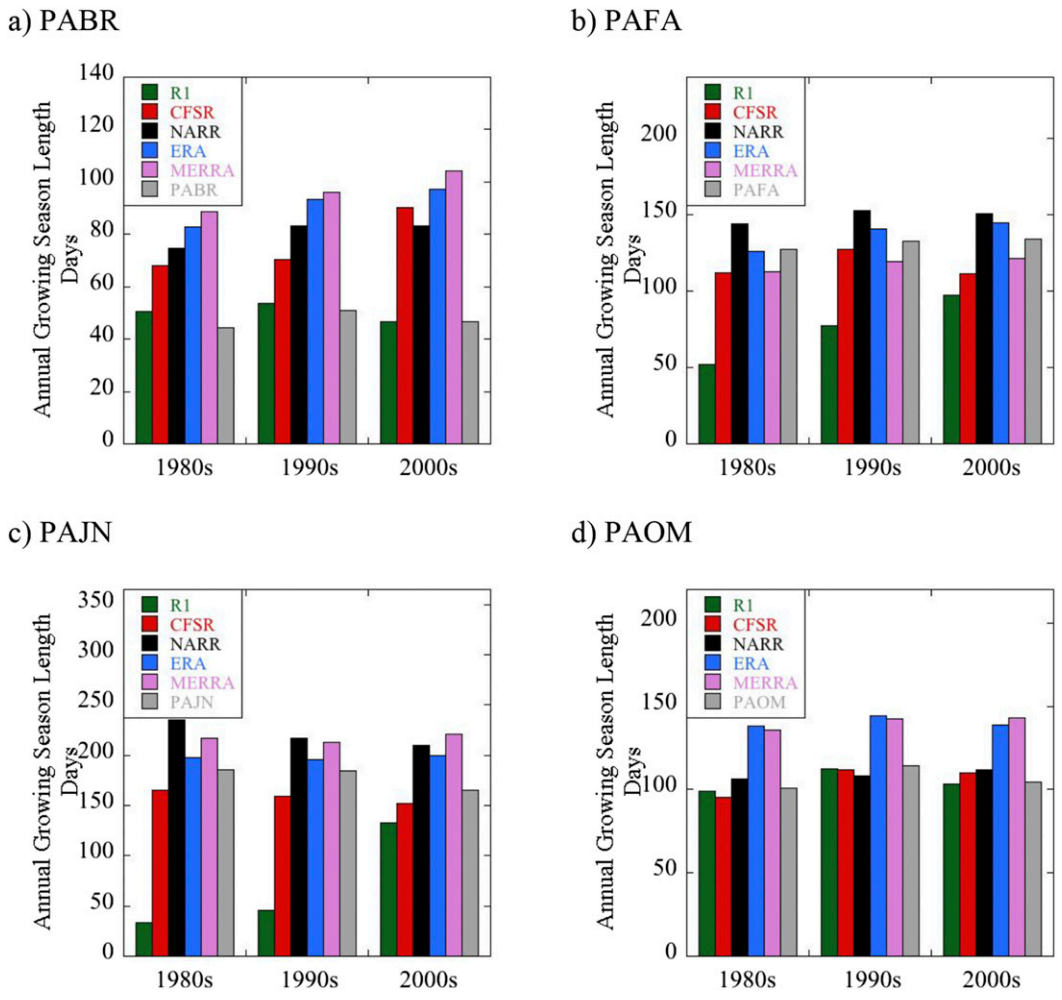

FIG. 11. Decadal-average annual counts of GSL at (a) Barrow, (b) Fairbanks, (c) Juneau, and (d) Nome. GSL represents the number of days between the fifth consecutive day when $T_{avg} > 0°C$ and the day when $T_{min} \leq -2.2°C$ for all stations.

and wide-ranging consequences to ecosystems, human health, and carbon storage. The typical wildfire season in Alaska begins in late spring and continues through midsummer before wetting rains end the season. Wildfire initiation and growth require heat, fuel, and a trigger (usually lightning).

ERA-Interim and MERRA display the lowest summer temperature bias in the Interior, whereas CFSR and MERRA do for the Cook Inlet zone (Table 1). At the station-gridpoint scale, these three reanalyses have comparably small biases for daily T_{min} during the late spring at both Fairbanks (Fig. 6b) and Anchorage (Fig. 6e). ERA-Interim exhibits large negative T_{max} bias (Figs. 5b,e), however, because of the mismatch between the station and nearest gridcell altitude in ERA-Interim for these locations (Fig. 2). The late summer (July–September) wetting rains are handled similarly well by all reanalyses except R1 (Fig. 7b), which produces too much precipitation. MERRA and ERA also display the best representation of extreme-precipitation days at Fairbanks (Fig. 10b), which is a relevant extremes index for late summer. Overall, MERRA is the recommended reanalysis for studying wildfire and related hazards in Alaska, but ERA-Interim is a quality choice for the Interior and CFSR is a good choice for the Cook Inlet zone.

Flash flooding and river flooding are major natural hazards in Alaska that can threaten lives and infrastructure almost immediately and, if severe enough, can cause long-lasting effects that extend to the relocation of entire villages. The mechanisms for flooding vary across the state. In the Interior, river flooding typically occurs in the late spring as the river ice melts, breaks up, and produces localized ice jams. Heavy summer precipitation can also cause Interior rivers to flood their banks. In the

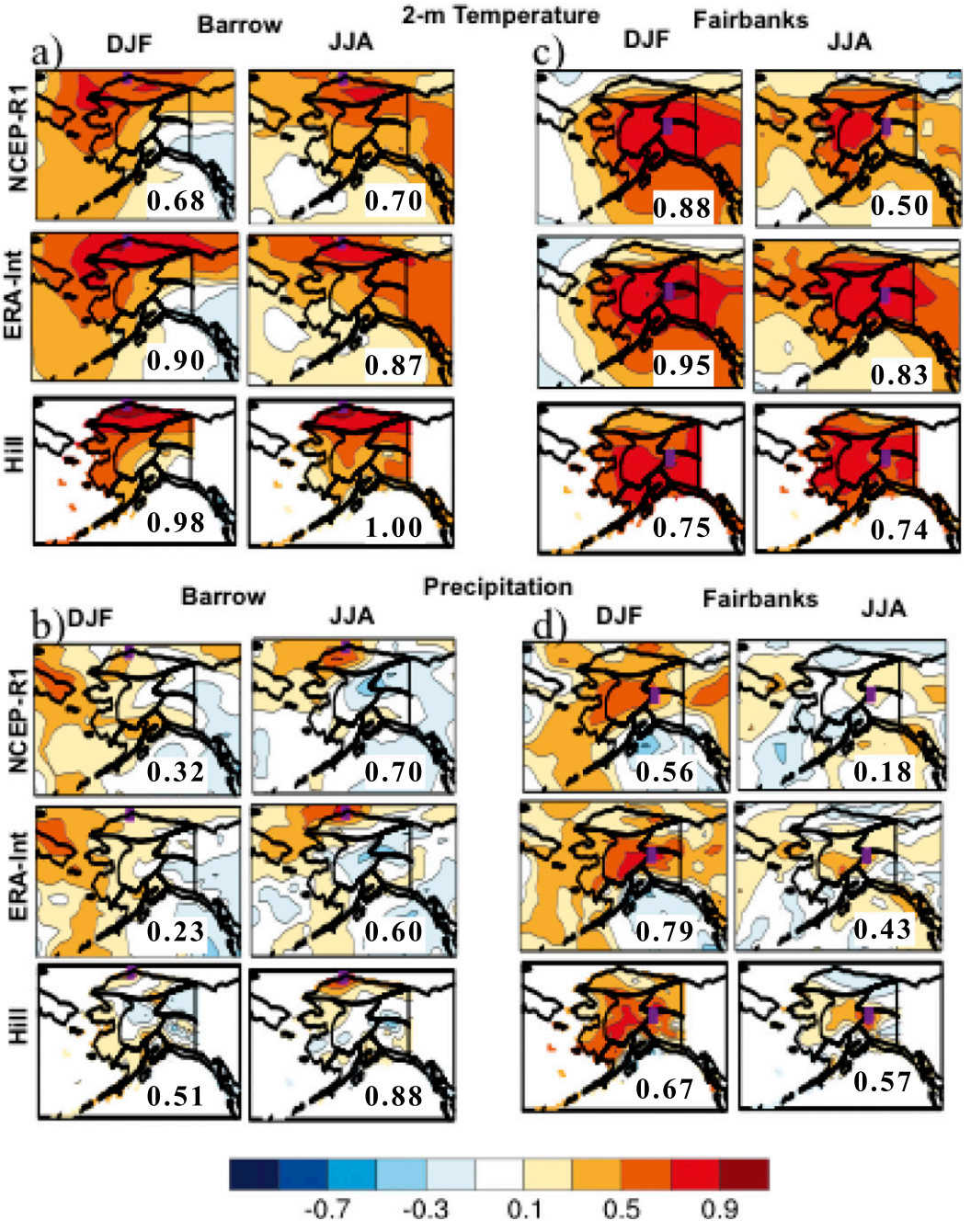

FIG. 12. Cross correlations between gridded datasets and station observations at Barrow for (a) temperature and (b) precipitation and at Fairbanks for (c) temperature and (d) precipitation. The latitudes and longitudes span 52°–72°N and 180°–210°E, respectively. The number in each map represents the correlation between the station data and the nearest grid point.

Southeast zone, extreme precipitation can occur from summer through winter across areas with steep terrain gradients and can induce landslides.

The key variables for Interior flooding are identical to those for wildfire but also include April temperature as an important indicator. As such, both MERRA and ERA-Interim are recommended reanalyses for impact studies that relate to Interior flooding and warm-season hydrology. Recall that MERRA resolves the Interior topography better than ERA-Interim (Figs. 2e,f) does, and this fact likely lowers its bias of daily T_{max} at the station-gridcell level.

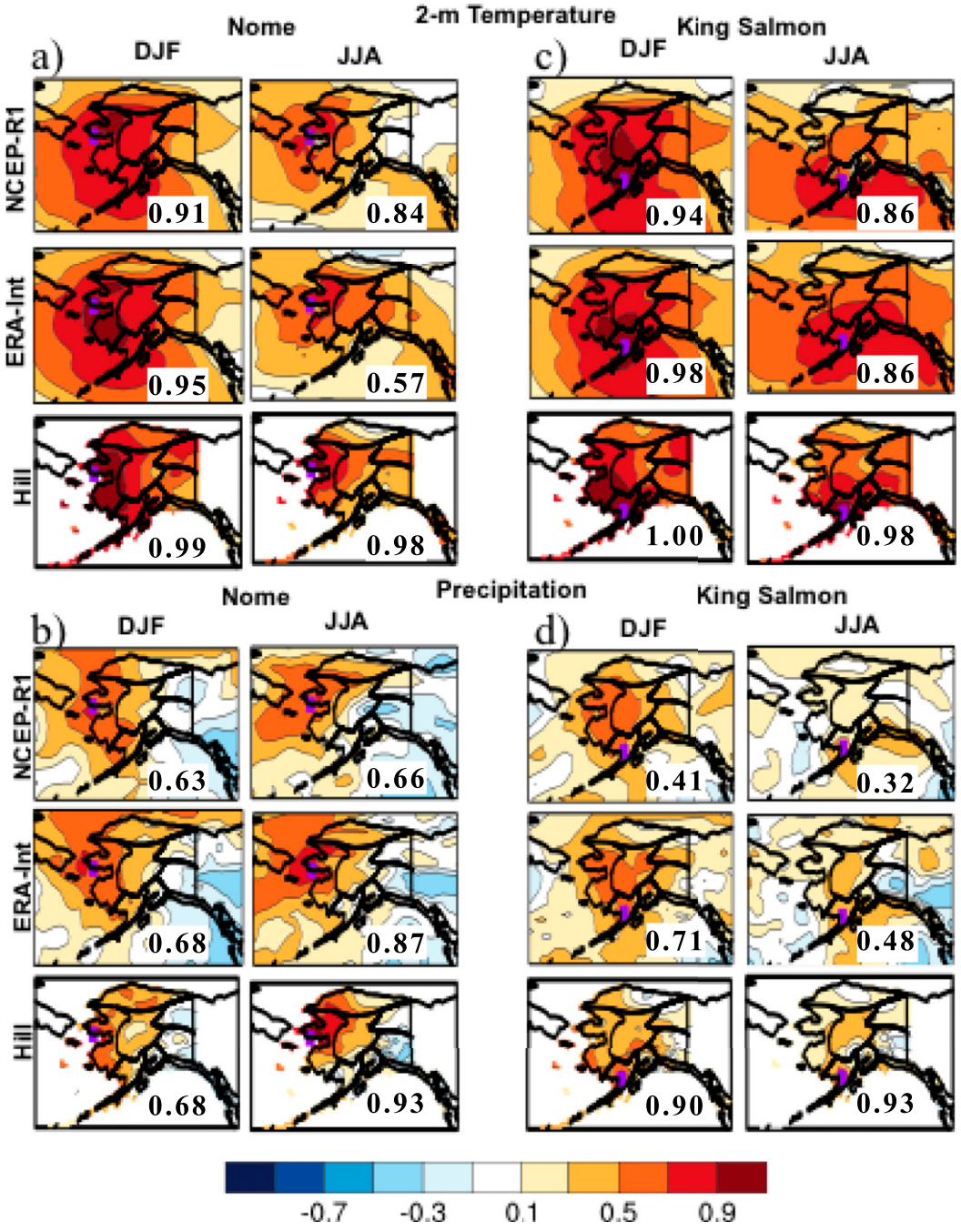

FIG. 13. As in Fig. 12, but for (a),(b) Nome and (c),(d) King Salmon.

In the Southeast zone, heavy precipitation can occur all year but is least likely in the spring. CFSR and ERA-Interim show the smallest summer and winter precipitation biases (Table 2) and are markedly closer to the spatially observed average than are the other three reanalyses, which are too dry. MERRA displays the best representation of EPD for Juneau, but because of the steep terrain gradients in this area the nearest-gridcell statistics should be used with caution.

A related hazard, and one that is potentially more devastating, is coastal erosion all around Alaska but along the Chukchi and Beaufort Seas in particular. Beginning in the late summer and continuing into early winter, deep low pressure centers traverse north through the Bering Sea and eastward across the Arctic Coast.

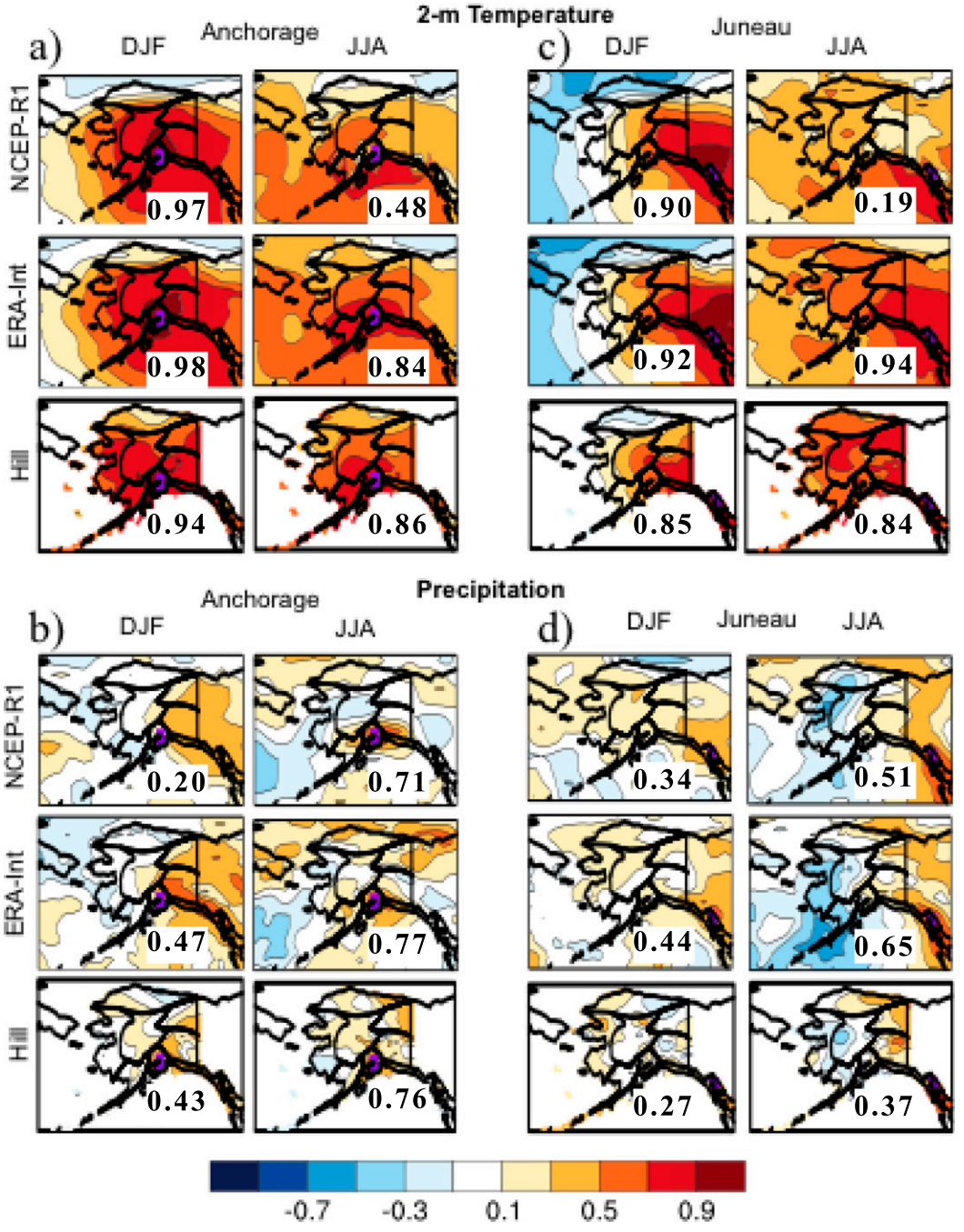

FIG. 14. As in Fig. 12, but for (a),(b) Anchorage and (c),(d) Juneau.

When there is sea ice to function as a buffer for the strong wind and wave action of the ocean, there is less of an impact. As these nearshore waters become increasingly ice free for longer periods, however, the danger from coastal erosion and flooding is magnified.

CFSR stands out among the reanalyses as having the most-stable (small) biases of daily T_{max} (Fig. 5a) and T_{min} (Fig. 6a) throughout the year for Barrow. Furthermore, during the ice-free summer season, CFSR displays a temperature bias of 0.0°C across the North Slope zone, which suggests that CFSR is the recommended reanalysis for zonewide climate-change applications. This discussion assumes that accurate depictions of temperature are necessary to resolve the sea ice fields and resultant hazard vulnerability. Note that coastal erosion is an important issue for the West Coast and

TABLE 3. Natural hazards in Alaska divided by climate zone. The top-performing reanalyses for each hazard are shown according to key meteorological variables and the months (in parentheses) during which these variables are most likely to affect the natural hazards.

Natural hazard	Climate zone	Key variables	Preferred reanalysis
Wildfire	Interior	Temperature (May–Aug); precipitation (Jul–Aug)	MERRA and ERA
Wildfire	Cook Inlet	Temperature (May–Aug); precipitation (Jul–Aug)	MERRA and CFSR
River flooding	Interior	Temperature (Apr–Aug); precipitation (Jun–Aug)	MERRA and ERA
Heavy precipitation	Southeast	Precipitation (Aug–Jan)	CFSR and ERA
Coastal erosion	North Slope	Temperature (Aug–Nov)	CFSR

Bristol Bay zones; no reanalysis in this study separates itself from the others in terms of performance for this hazard in these zones, however. Future studies should include winds and storminess to provide a more comprehensive analysis.

It is admitted that this synthesis leaves out many hazards for Alaska and that the ones that are included are limited to an assessment using solely temperature and precipitation. Permafrost degradation is an enormous threat to the Alaskan way of living, not to mention its global effect on the concentration of methane in the atmosphere; inclusion of a snow variable would be necessary to assess reanalysis performance with respect to this hazard, however. Change to specific wildlife habitat is another key issue that is not covered in this synthesis, but examples that are included provide the reader, and the users of these reanalysis data, with guidance on how to identify key variables for their studies and to make informed selections from available reanalyses for use in decision making, forcing of offline models, or other applications.

Acknowledgments. We thank Igor Polyakov for fruitful discussions and three anonymous reviewers for their thoughtful comments that improved this paper. This work was made possible through financial support from the Alaska Climate Science Center, funded by Cooperative Agreement G10AC00588 from the U.S. Geological Survey. Its contents are solely the responsibility of the author and do not necessarily represent the official view of the USGS. Support for John Walsh was provided by the NOAA Climate Program Office through Grant NA11OAR4310141 to the Alaska Center for Climate Assessment and Policy.

REFERENCES

Bekryaev, R. V., I. V. Polyakov, and V. A. Alexeev, 2010: Role of polar amplification in long-term surface air temperature variations and modern Arctic warming. *J. Climate*, **23**, 3888–3906, doi:10.1175/2010JCLI3297.1.

Bieniek, P. A., U. S. Bhatt, L. A. Rundquist, S. D. Lindsey, X. Zhang, and R. L. Thoman, 2011: Large-scale climate controls of interior Alaska river ice breakup. *J. Climate*, **24**, 286–297, doi:10.1175/2010JCLI3809.1.

——, and Coauthors, 2012: Climate divisions for Alaska based on objective methods. *J. Appl. Meteor. Climatol.*, **51**, 1276–1289, doi:10.1175/JAMC-D-11-0168.1.

Bosilovich, M. G., 2008: NASA's Modern Era Retrospective-Analysis for Research and Applications: Integrating Earth observations. *IEEE Earthzine*, **1** (1–4), 82367. [Available online at http://www.earthzine.org/2008/09/26/nasas-modern-era-retrospective-analysis/.]

Brönnimann, S., A. N. Grant, G. P. Compo, T. Ewen, T. Griesser, A. M. Fischer, M. Schraner, and A. Stickler, 2012: A multi-data set comparison of the vertical structure of temperature variability and change over the Arctic during the past 100 years. *Climate Dyn.*, **39**, 1577–1598, doi:10.1007/s00382-012-1291-6.

Chapin, F. S., III, S. F. Trainor, P. Cochran, H. Huntington, C. Markon, M. McCammon, A. D. McGuire, and M. Serreze, 2014: Alaska. *Climate Change Impacts in the United States: The Third National Climate Assessment*, J. M. Melillo, T. C. Richmond, and G. W. Yohe, Eds., U.S. Global Change Research Program, 514–536. [Available online at http://nca2014.globalchange.gov/system/files_force/downloads/high/NCA3_Full_Report_22_Alaska_HighRes.pdf?download=1.]

Cullather, R. I., and M. G. Bosilovich, 2011: The moisture budget of the polar atmosphere in MERRA. *J. Climate*, **24**, 2861–2879, doi:10.1175/2010JCLI4090.1.

Daly, C., R. P. Neilson, and D. L. Phillips, 1994: A statistical-topographic model for mapping climatological precipitation over mountainous terrain. *J. Appl. Meteor.*, **33**, 140–158, doi:10.1175/1520-0450(1994)033<0140:ASTMFM>2.0.CO;2.

Dee, D. P., and Coauthors, 2011: The ERA-Interim reanalysis: Configuration and performance of the data assimilation system. *Quart. J. Roy. Meteor. Soc.*, **137**, 553–597, doi:10.1002/qj.828.

Ek, M. B., K. E. Mitchell, Y. Lin, E. Rogers, P. Grunmann, V. Koren, G. Gayno, and J. D. Tarpley, 2003: Implementation of Noah land surface model advances in the National Centers for Environmental Prediction operational mesoscale Eta Model. *J. Geophys. Res.*, **108**, 8851, doi:10.1029/2002JD003296.

Fan, X., J. E. Walsh, and J. R. Krieger, 2008: A one-year experimental Arctic reanalysis and comparisons with ERA-40 and NCEP/NCAR reanalyses. *Geophys. Res. Lett.*, **35**, L19811, doi:10.1029/2008GL035110.

Francis, O. P., and D. E. Atkinson, 2012: Synoptic forcing of wave states in the southeast Chukchi Sea, Alaska, at nearshore locations. *Nat. Hazards*, **62**, 1273–1300, doi:10.1007/s11069-012-0148-y.

Hartmann, B., and G. Wendler, 2005: The significance of the 1976 Pacific climate shift in the climatology of Alaska. *J. Climate*, **18**, 4824–4839, doi:10.1175/JCLI3532.1.

Hayhoe, K. A., 2010: A standardized framework for evaluating the skill of regional climate downscaling techniques. Ph.D. dissertation, University of Illinois at Urbana–Champaign, 158 pp. [Available online at http://www.snap.uaf.edu/attachments/1_Hayhoe_Katharine.pdf.]

Hill, D. F., N. Bruhis, S. E. Calos, A. Arendt, and J. Beamer, 2015: Spatial and temporal variability of freshwater discharge into the Gulf of Alaska. *J. Geophys. Res.*, **120**, 634–646, doi:10.1002/2014JC010395.

Kalnay, E., 2003: *Atmospheric Modeling, Data Assimilation, and Predictability*. Cambridge University Press, 341 pp.

——, and Coauthors, 1996: The NCEP/NCAR 40-Year Reanalysis Project. *Bull. Amer. Meteor. Soc.*, **77**, 437–471, doi:10.1175/1520-0477(1996)077<0437:TNYRP>2.0.CO;2.

Karl, T. R., N. Nicholls, and A. Ghazi, 1999: CLIVAR/GCOS/WMO workshop on indices and indicators for climate extremes: Workshop summary. *Climatic Change*, **42**, 3–7, doi:10.1023/A:1005491526870.

Kistler, R., and Coauthors, 2001: The NCEP–NCAR 50-Year Reanalysis: Monthly means CD-ROM and documentation. *Bull. Amer. Meteor. Soc.*, **82**, 247–267, doi:10.1175/1520-0477(2001)082<0247:TNNYRM>2.3.CO;2.

Lindsay, R., M. Wensnahan, A. Schweiger, and J. Zhang, 2014: Evaluation of seven different atmospheric reanalysis products in the Arctic. *J. Climate*, **27**, 2588–2606, doi:10.1175/JCLI-D-13-00014.1.

Mernild, S. H., G. E. Liston, and C. A. Hiemstra, 2014: Northern Hemisphere glacier and ice caps surface mass balance and contribution to sea level rise. *J. Climate*, **27**, 6051–6073, doi:10.1175/JCLI-D-13-00669.1.

Mesinger, F., and Coauthors, 2006: North American Regional Reanalysis. *Bull. Amer. Meteor. Soc.*, **87**, 343–360, doi:10.1175/BAMS-87-3-343.

Mills, C. M., and J. E. Walsh, 2013: Seasonal variation and spatial patterns of the atmospheric component of the Pacific decadal oscillation. *J. Climate*, **26**, 1575–1594, doi:10.1175/JCLI-D-12-00264.1.

Parrish, D. F., and J. C. Derber, 1992: The National Meteorological Center's spectral statistical-interpolation analysis system. *Mon. Wea. Rev.*, **120**, 1747–1763, doi:10.1175/1520-0493(1992)120<1747:TNMCSS>2.0.CO;2.

Pickart, R. S., A. M. Macdonald, G. W. K. Moore, I. A. Renfrew, J. E. Walsh, and W. S. Kessler, 2009: Seasonal evolution of Aleutian low pressure systems: Implications for the North Pacific subpolar circulation. *J. Phys. Oceanogr.*, **39**, 1317–1339, doi:10.1175/2008JPO3891.1.

Pithan, F., and T. Mauritsen, 2013: Comments on "Current GCMs' unrealistic negative feedback in the Arctic." *J. Climate*, **26**, 7783–7788, doi:10.1175/JCLI-D-12-00331.1.

Rienecker, M. M., and Coauthors, 2011: MERRA: NASA's Modern-Era Retrospective Analysis for Research and Applications. *J. Climate*, **24**, 3624–3648, doi:10.1175/JCLI-D-11-00015.1.

Rodionov, S. N., J. E. Overland, and N. A. Bond, 2005: The Aleutian low and winter climatic conditions in the Bering Sea. Part I: Classification. *J. Climate*, **18**, 160–177, doi:10.1175/JCLI3253.1.

Ruane, A. C., 2010: NARR's atmospheric water cycle components. Part I: 20-year mean and annual interactions. *J. Hydrometeor.*, **11**, 1205–1219, doi:10.1175/2010JHM1193.1.

Rupp, T. S., X. Chen, M. Olson, and D. A. McGuire, 2007: Sensitivity of simulated boreal fire dynamics to uncertainties in climate drivers. *Earth Interact.*, **11**, 1–21, doi:10.1175/EI189.1.

Saha, S., and Coauthors, 2010: The NCEP Climate Forecast System Reanalysis. *Bull. Amer. Meteor. Soc.*, **91**, 1015–1057, doi:10.1175/2010BAMS3001.1.

Shulski, M., J. Walsh, E. Stevens, and R. Thoman, 2010: Diagnosis of extended cold-season temperature anomalies in Alaska. *Mon. Wea. Rev.*, **138**, 453–462, doi:10.1175/2009MWR3039.1.

Smith, C. A., G. P. Compo, and D. K. Hooper, 2014: Web-Based Reanalysis Intercomparison Tools (WRIT) for analysis and comparison of reanalyses and other datasets. *Bull. Amer. Meteor. Soc.*, **95**, 1671–1678, doi:10.1175/BAMS-D-13-00192.1.

Uppala, S. M., and Coauthors, 2005: The ERA-40 Re-Analysis. *Quart. J. Roy. Meteor. Soc.*, **131**, 2961–3012, doi:10.1256/qj.04.176.

Xie, P., and P. A. Arkin, 1997: Global precipitation: A 17-year monthly analysis based on gauge observations, satellite estimates, and numerical model outputs. *Bull. Amer. Meteor. Soc.*, **78**, 2539–2558, doi:10.1175/1520-0477(1997)078<2539:GPAYMA>2.0.CO;2.

Yang, D., B. E. Goodison, J. R. Metcalfe, V. S. Golubev, R. Bates, T. Pangburn, and C. L. Hanson, 1998: Accuracy of NWS 8″ standard nonrecording precipitation gauge: Results and application of WMO intercomparison. *J. Atmos. Oceanic Technol.*, **15**, 54–68, doi:10.1175/1520-0426(1998)015<0054:AONSNP>2.0.CO;2.